Draft version May 27, 2021
Typeset using LaTeX default style in AASTeX63

p-Mode Oscillations in Gravitationally Highly Stratified Magnetic Solar Atmospheres

M. Griffiths,[1] R. Erdélyi,[2,3,4] R. Zheng,[5] and N. Gyenge[1]

[1] *Research IT, The University of Sheffield, 10-12 Brunswick Street, Sheffield, S10 2FN, UK.*
[2] *Solar Physics and Space Plasma Research Centre (SP^{2}RC), School of Mathematics and Statistics, University of Sheffield, Hicks Building, Hounsfield Road, S7 3RH, UK*
[3] *Department of Astronomy, Eötvös Loránd University, Pázmány P. sétány 1/A, Budapest, H-1117, Hungary*
[4] *Gyula Bay Zoltán Solar Observatory (GSO), Hungarian Solar Physics Foundation (HSPF), Petőfi tér 3., Gyula, H-5700, Hungary*
[5] *Shandong Key Laboratory of Optical Astronomy and Solar-Terrestrial Environment, School of Space Science and Physics, Institute of Space Sciences, Shandong University, Weihai, Shandong, 264209, China*

(Received June 1, 2019; Revised January 10, 2019; Accepted May 27, 2021)

Submitted to AJ

ABSTRACT

The aim of the work reported in this paper is to gain understanding of the propagation characteristics of p-mode oscillations in the highly gravitationally stratified magnetic solar atmosphere. An objective is the measurement of the properties of the solar atmosphere and its magnetic structures. We present a comparison of the analysis of results from observations and numerical simulations.

The paper describes 3D numerical magnetohydrodynamic (MHD) simulations of a model solar atmosphere with a uniform vertical cylindrically symmetric magnetic field and employing simulation drivers resulting in oscillations which mimic the behaviour of p-mode oscillations. The simulations were run for different values of the magnitude of the magnetic field and a p-mode driver with a fixed period of 300 s. For the observational study, a typical active region was selected. Temporal analysis of the observational data for the region containing a small sunspot (solar pore).

The paper reports the variation of the energy flux and oscillation frequency of the magnetosonic modes and examines their dependence on the magnetic field strength. Comparison with observational data indicate the presence of oscillation signals with a frequency close to that measured for the simulated results.

We conclude that magnetic regions of the solar atmosphere are favourable regions for the propagation of energy by slow magnetosonic modes. The results exhibit a frequency shift, for different values of the magnetic field. The obtained periodic behaviour is confirmed by observational data, featuring similar frequencies based on the intensity times series of images taken by the Solar Dynamics Observatory.

Keywords: editorials, notices — miscellaneous — catalogs — surveys

1. INTRODUCTION

Observational, theoretical and computational studies of the Sun's atmosphere reveal a diversity of structures and complex dynamics. This is clearly revealed by imagery from solar telescopes. The culmination of studies of the dynamics of the coronal loop structures in the upper solar atmosphere and in the solar chromosphere has developed our understanding of the range of different magnetic field structures. Despite our armoury of observations and diverse range of computational models it still remains a challenge to make sense of this complex menagerie of dynamical structures, understand solar atmospheric (i.e. chromospheric and coronal) heating and more generally space weather phenomena.

Corresponding author: M. Griffiths
m.griffiths@sheffield.ac.uk

An example of the dynamical complexity are the ubiquitous five-minute oscillations in the solar atmosphere that are referred to as the solar global acoustic oscillations or p-modes. These global oscillations are interpreted as trapped acoustic waves, i.e. standing acoustic oscillations of the solar interior. The solar p-modes also perturb the photosphere, and the main restoring force for these acoustic oscillations is kinetic pressure. Earlier models had assumed reflection at the photosphere, and at most allowed evanescence above the photosphere. There is now increasing evidence for leakage of these modes. The p-modes were seen as resonant modes between the steep change in density at the solar surface and trapped beneath by the increase of the sound speed causing refraction and eventually forming a lower turning point in the interior. The observation of the resulting standing modes are now widely used as a diagnostic tool to estimate the physical characteristics of the solar sub-surface layers.

The complexity and variety of magnetic structures in the solar atmosphere give rise to a mixture of waves providing powerful diagnostics to aid our understanding and advance our knowledge. The characteristics of generated waves is dependent on the motions at the footpoints of magnetic field concentrations and includes those in the intergranular lanes. For example vortex motions have been demonstrated to generate Alfvén waves Fedun et al. (2009b).

In this paper, we report the results of numerical simulations of photospheric p-mode oscillations in a model solar atmosphere with a uniform and vertical magnetic field. First, we consider the variety of magnetic structures in the solar atmosphere and address the wave motions that are observed in these regions. This is followed with a description of the solar atmospheric model, magnetic field configuration and the simulation method we used to model p-mode oscillations in a model magnetic solar atmosphere.

2. STRUCTURES IN THE SOLAR ATMOSPHERE

The highly dynamic solar chromosphere exhibits many different kinds of structures. For example faculae, pores or the bright areas near to and around sunspots. Pores are smaller counterparts of sunspots up to a few Mm across. The faculae are bright spots forming in the trenches between solar granules, they constantly form and dissipate over time scales of several minutes and they are formed near magnetic field concentrations. The bright areas that extend away from active regions are called plage regions. The magnetic fields in this area diffuse away into the quiet Sun regions. The magnetic network is a network of lines which outline super-granules. The super-granule are convective regions about 30 Mm across, and they possess strong horizontal flows. The motions within the super-granules result in the concentration of bundles of magnetic field lines. The mean photospheric field in the inter-network region is 100-300 G. On the other hand, solar active regions contain sunspots which have sizes between 1 - 50 Mm.

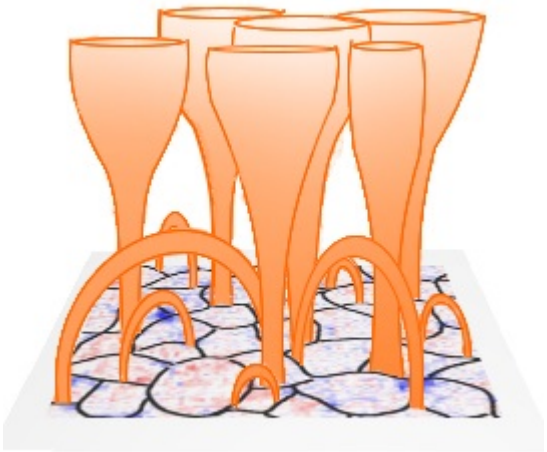

Figure 1. The schematic solar magnetic network.

Active regions producing flares may have fields which easily exceed the normal range of 100-500 G. As well as these massive concentrations, solar magnetograms reveal many north poles in the quiet photosphere, this is known as the magnetic carpet. These structures can be observed in figure 1. Along with the coronal funnels arising from grain boundaries, the picture shows a range of network loops with temperatures which can be in the range 10^5K to 10^6K.

The dynamical phenomena of concern in this paper result in waves and oscillations in the solar atmosphere. The upward propagation of waves through the solar atmosphere can result in coronal heating, frequency shifts and other wave phenomena. A range of wave transformations may occur including reflection and refraction by atmospheric structures. Our initial studies were relevant for the quiet inter-network region of the non magnetic solar chromosphere, which is similar to the quiet sun with magnetic fluxes in the range 5-10G. These are the regions between the magnetic flux concentrations.

Given this variety of solar regions it is recognised that the modes of oscillation with periods of 3 and 5 minutes behave in different ways in the solar atmosphere network, inter network, plage and faculae regions. What is striking is the varied behaviour for different magnetic structures and the influence of reflecting layers such as the transition layer influencing upward and downward propagation. The power spectra presented in the first figure of Griffiths et al. (2018b) exhibit a variation of propagation characteristics at different levels within the solar atmosphere and within different regions such as coronal holes, the quiet sun and active regions. In general the power spectra indicate a preponderance of long period 5 minute waves with frequencies in the range 1.5-5mHz. Also observed are the distinctive peaks for the short period 3 minute waves (with frequencies in the range 5-8mHz). The power spectra exhibit peaks in much longer period ranges for example 12 minute waves (frequencies in the range 1.1-1.5mHz) and 16 minute waves (frequencies 1-1.1mHz). For the quiet sun regions the 5 minute modes are stronger at photospheric levels and diminished higher up in the corona, but note a small peak for the AIA 211 corresponding to 2.0MK.

The review of Khomenko and Calvo Santamaria (2013) summarises this complex picture. For the network and inter network regions the short period 3 minute modes propagate from the photosphere to the chromosphere only in restricted areas of the network cell interiors. The longer 5 minute modes propagate efficiently to the chromosphere in the close proximity of the magnetic network elements. These long-period network halos are most prominent in the photosphere, but are also present in the chromosphere; and are observed to be co-spatial with chromospheric "magnetic shadows" for 3 min waves. The plage and faculae regions possess more complex magnetic structures and exhibit a more complex pattern. Observations show that the power of the 5 minute modes increase significantly in the chromosphere. For the short period 3 minute modes there is an enhancement, both in the photosphere and in the chromosphere. These power enhancements are known as "halos" and have been widely reported Kontogiannis et al. (2010).

3. MOTIVATION

Given the complexity of the dynamics and the diversity of structures in the solar atmosphere. It is understood that a truly realistic model is challenging requiring a hybrid multi-disciplined approach. In order to develop a model providing a representation of the solar atmosphere it is necessary to establish that the modelling tools give a consistent behaviour in idealised test cases and that there is a consistency between the computational and theoretical models. Many computational MHD simulations of the sun have been undertaken some of the approaches have resulted in an encouraging degree of realism Vögler et al. (2005), Gudiksen et al. (2011). Computational MHD simulations of the propagation of waves in 3D solar atmospheres was undertaken by Fedun et al. (2009a). Initially they considered hydrodynamical models, in later simulations Fedun et al. (2009b) Vigeesh et al. (2012) reported results for magnetized solar atmospheres featuring an idealized flux tube. These models with point drivers demonstrated the leakage of magneto-acoustic energy into the solar atmosphere. The work of Khomenko and Calvo Santamaria (2013) and Calvo Santamaria, Khomenko and Collados (2015) reviewed and presented 2D computational MHD modelling of wave propagation in magnetic features such as sunspots and arcades. Such models reveal that energy reaches the corona along vertical magnetic fields.

Our initial models were hydrodynamic simulations of a realistically stratified model of the solar atmosphere representing its lower region from the photosphere to low corona Griffiths et al. (2018b). The objective was to model atmospheric perturbations, propagating from the photosphere into the chromosphere, transition region and low corona. The perturbations caused by the photospheric global oscillations were represented in the simulations using photospheric drivers to mimic the solar p-modes. These hydrodynamic modelling studies demonstrated that the energy flux predictions were in agreement with the results of the two layer Klein-Gordon model supporting our interpretation of the interaction of solar global oscillations with the solar atmosphere.

The simulations also revealed a consistency between the frequency-dependence of the energy flux in the numerical simulations and power flux measurements obtained from SDO and demonstrated the propagation of energy into the mid- to upper-atmosphere of the quiet Sun, this occured for a range of frequencies and may explain observed intensity

oscillations for periods greater than the well known 3-minute and 5-minute oscillations. It was also found that energy flux propagation into the lower solar corona is strongly dependent on the particular wave modes.

In this paper we present results for 3D numerical MHD simulations with an extended driver representing photospheric p-mode oscillations in a magnetic solar atmosphere, the objective is to gain understanding of the propagation characteristics of the p-mode oscillations.

4. NUMERICAL COMPUTATION METHODS

The 3D numerical simulations described here were undertaken using: Sheffield MHD Accelerated Using GPUs (SMAUG) Griffiths et al. (2015), the GPU implementation of the Sheffield Advanced Code (SAC) Shelyag et al. (2008). SAC and SMAUG are numerical MHD solvers allowing us to model the time-dependent evolution of photospheric oscillations in the solar atmosphere. SAC is a derivative of the versatile advection code (VAC) developed by (Tóth 1996). The general system of ideal MHD equations are

$$\frac{\partial \rho}{\partial t} + \nabla \cdot (\rho \mathbf{v}) = 0, \tag{1}$$

$$\frac{\partial (\rho \mathbf{v})}{\partial t} + \nabla \cdot (\mathbf{v}\rho\mathbf{v} - \mathbf{B}\mathbf{B}) + \nabla p_t = \rho \mathbf{g}, \tag{2}$$

$$\frac{\partial e}{\partial t} + \nabla \cdot (\mathbf{v}e - \mathbf{B}\mathbf{B} \cdot \mathbf{v} + \mathbf{v}p_t) + \nabla p_t = \rho \mathbf{g} \cdot \mathbf{v}, \tag{3}$$

$$\frac{\partial \mathbf{B}}{\partial t} + \nabla \cdot (\mathbf{v}\mathbf{B} - \mathbf{B}\mathbf{v}) = 0. \tag{4}$$

Here, ρ is the mass density, $\mathbf{v}$ is the velocity, $\mathbf{B}$ is the magnetic field, e is the energy density, p_t is the total pressure and $\mathbf{g}$ is the gravitational acceleration vector. The total pressure p_t is written as

$$p_t = p_k + \frac{\mathbf{B}^2}{2}, \tag{5}$$

where p_k is the kinetic pressure given by

$$p_k = (\gamma - 1)\left(e - \frac{\rho \mathbf{v}^2}{2} - \frac{\mathbf{B}^2}{2}\right). \tag{6}$$

Equations (1) - (6) are applicable to an ideal compressible plasma. The SAC code is based on perturbed versions of these equations, thus the variables ρ, e and $\mathbf{B}$ are expressed in terms of perturbed and background quantities as

$$\rho = \tilde{\rho} + \rho_b,$$
$$e = \tilde{e} + e_b,$$
$$\mathbf{B} = \tilde{\mathbf{B}} + \mathbf{B}_b.$$

where $\tilde{\rho}$ is the perturbed density, $\tilde{e}$ is the perturbed energy and $\tilde{\mathbf{B}}$ is the perturbed magnetic field. The background quantities with a subscript b do not change in time, as we assume a magneto-hydrostatic equilibrium of the background plasma.

The SMAUG code is a fully non-linear MHD numerical finite element solver for simulating, linear and non-linear wave propagation in strongly magnetised plasma with structuring and stratification. The solver applies a fourth order central differencing technique to the spatial derivatives and the Euler or fourth order Runge-Kutta method to solve the temporal derivatives. By virtue of their symmetry, central differencing schemes are conservative, with the desired side effect that the solver conserves the divergence of the magnetic field. The application of central differencing to hyperbolic differential equations results in unstable solutions with a spurious oscillatory behaviour.

Hyper-diffusion and hyper-resistivity are implemented to achieve numerical stability of the computed solution of the MHD equations (see for example Caunt and Korpi 2001). The primary purpose of the diffusion terms is to compensate for the anti-diffusion from truncation errors arising in the computation of temporal and spatial derivatives. When the diffusion is correctly tuned the resulting evolution is non-diffusive. In addition, the diffusion terms control the steepness of shocks by becoming large wherever the compression is large. The full set of MHD equations, including the hyper-diffusion source terms are given in Griffiths et al. (2015) and Shelyag et al. (2008).

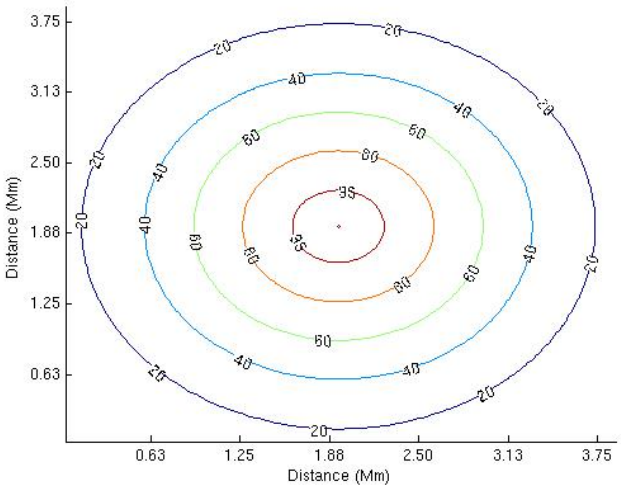

Figure 2. Initial Magnetic Field Configuration, radial field distribution, uniform in the vertical direction with a maximum value of 100G

5. COMPUTATIONAL MODEL

The computational box used for our simulations represents a volume of the solar atmosphere with dimensions $L_x = 4$ Mm and $L_y = 4$ Mm. The model utilises a representation of the solar atmosphere with gravitational stratification in the z-direction and with a height of $L_z = 6$ Mm. The computational box comprises an array of elements of dimension $128 \times 128 \times 128$. The upper boundary of our model is in the solar corona and the lower boundary in the photosphere. The SMAUG code is well suited for modelling the leakage of wave energy from the photosphere, through the transition region and into the corona. We used open boundary conditions for all of the boundaries, allowing the modelling of wave propagation for time scales characterised by the 5-minute p-mode induced oscillations. The computational model is excited by an extended vertical velocity driver located at the photosphere, this acoustic p-mode driver excites waves which propagate into a realistic 3D model of the solar atmosphere. In the following two sections we describe the solar atmospheric model and the implementation of the driver.

For the hydrodynamical studies reported in Griffiths et al. (2018b), simulation drivers were used which behave like p-mode oscillations with varying modes and periods. We performed MHD simulations using our model of the solar atmosphere and including a uniform vertical cylindrically symmetric magnetic field.

The model atmosphere employed here is an observationally derived semi-empirical representation of the quiet sun. With the fundamental assumption of hydrostatic equilibrium a model of the chromosphere in equilibrium is constructed using the VALIIIc model, see Vernazza et al. (1981). For the region of the solar atmosphere above 2.5 Mm the results of the energy balance model of solar coronal heating has been used (see McWhirter et al. 1975), his model includes an acoustic contribution comparable to the hydrostatic pressure. An option is the use of a parametrisation of the temperature of the solar atmosphere which may be a smoothed step function profile see Murawski and Zaqarashvili (2010). Results have demonstrated the need for observationally derived semi-empirical models of the solar atmosphere. There is much discussion about model validity and the work undertaken to demonstrate the reliability of the assumptions used to construct realistic models of the solar chromosphere, see Carlsson and Stein (1995), Kalkofen (2012). The contention arises from the dynamical nature of the solar chromosphere; for example local dynamo action has been suggested as a mechanism of Joule heating in the solar chromosphere, see Leenaarts et al. (2011).

A hydrostatic model for the solar atmosphere can be constructed by making use of the ideal gas equation for the solar atmosphere.

$$p_0 = \frac{\rho_0 R_{gas} T_0}{\mu}, \tag{7}$$

R_{gas} is the gas constant and μ is mean atomic weight. For the fully ionized higher region of the atmosphere $\mu = 0.5$, whilst lower down we set $\mu = 1$. p_0, ρ_0 and T_0 are the pressure, density and temperature distributions for the stratified

solar atmosphere. The scale height for the atmosphere is

$$H(z) = \frac{R_{gas} T_0(z)}{g}, \tag{8}$$

By using the scale height with the temperature profile from the VALIIIc and McWhirter model, the pressure equation is integrated over the atmospheric height and the density profile was computed.

$$\frac{dp_0(z)}{dz} = -\rho_0 g, \tag{9}$$

Illustrations of the resulting temperature and density profiles can be seen in Figure 2 of Griffiths et al. (2018b). For the simulations described here we use a simplistic model which is uniform in the vertical (z) direction. The cylindrically symmetric field was constructed using the parametrisation in equation 10. For the simulations here the effective cylinder radius is fixed at $R = 0.5Mm$, simulations were run for different values of B_{max}.

$$B_z = B_{max} e^{-\frac{x^2+y^2}{R^2}}, \tag{10}$$

Where $R = 0.25Mm$ Magnetic field model for solar atmosphere. Since the field is uniform in the vertical direction the model atmosphere in hydrostatic equilibrium is in magnetohydrostatic equilibrium.

6. NUMERICAL DRIVERS FOR *P*-MODE OSCILLATIONS

The overview of studies described in Section 2 identified a range of physical phenomena resulting in oscillatory behaviour and delivering energy into the solar atmosphere. Using drivers characterising the solar global oscillations, we extend the earlier work undertaken by Malins (2007), for their study, point drivers were used to represent periodic buffeting of turbulent motions in the photosphere. The results of the study demonstrated surface waves and structures in the transition region and highlighted the characteristics of the oscillatory phenomena as a result of frequency cut-offs induced by the stratified solar atmosphere. For the simulations presented in this paper, the whole boundary of the model was perturbed. In the real Sun, photospheric *p*-mode oscillations have a horizontal wavelength and coherence. For the simulations reported here, the excitations are represented with a vertical velocity driver located at the photosphere. This acoustic *p*-mode driver excites waves which propagate into a realistic 3D model of the solar atmosphere. Simulations were run with drivers representing different modes. For example, an extended driver with a sinusoidal dependence and a wavelength of 8 Mm applied along the middle of the base of a computational domain of dimension 4 Mm represents a *fundamental mode*. A driver with wavelength 4 Mm applied the same way represents the *first harmonic* and *second harmonic* with wavelength 2 Mm was also considered. Drivers may be constructed as an ensemble of these solar global eigenmodes. The driver is represented by the expression shown in equation (6)

$$\begin{aligned} V_z &= A_{nm} \sin\left(\frac{2\pi t}{T_s}\right) \sin\left(\frac{(n+1)\pi x}{L_x}\right) \times \\ &\quad \sin\left(\frac{(m+1)\pi y}{L_y}\right) \exp\left(-\frac{(z-z_0)^2}{\Delta z^2}\right), \end{aligned}$$

Simulations were run for different values of the magnitude of the magnetic field. For all of the simulations a p-mode driver was used with period 300s and mode (2,2). The 300s driver was used as this corresponds to the well known 5 minute mode. The (2,2) mode was used because our earlier study demonstrated its effectiveness with energy propagation. The mode numbers identified here are the n and m values in the expression for the driver shown in equation (6).

In equation (6) L_x and L_y are the lengths of the base of the simulation box in the x and y directions respectively. T_s is the period and A_{nm} is the amplitude of the driver, the indices n and m define the mode. Δz is the width of the driver which was set here to $4km$, the parameter z_0 was set so that the vertical driver location is coincident with the location of the temperature minimum which is 0.5 Mm above the lower boundary of the model i.e. the photosphere. The simulations presented use the parameter A_{nm}=500 ms^{-1} with the mode indices set to $n, m = 2$.

7. MAGNETOACOUSTIC WAVES IN UNIFORM VERTICAL MAGNETIC FIELD CONFIGURATIONS

Magnetohydrodynamic simulations have been performed with p-mode oscillations of the photospheric layer and for magnetic field strengths of 0G, 50G, 75G and 100G. The plasma β for the model decreases rapidly from a value of 12 at the lower boundary of the simulation domain. β decrease to 1 at 0.5Mm above the box boundary. From the top of

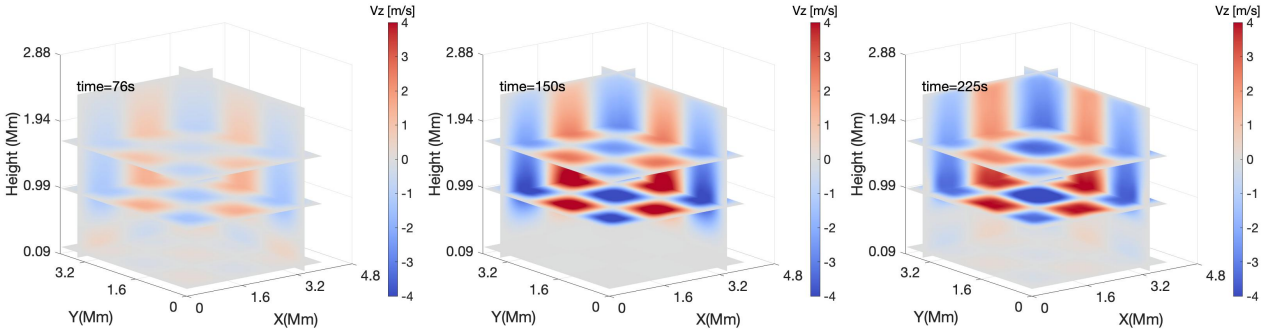

Figure 3. Vertical Component of the Velocity for Different Sections of the Simulation for 76s, 150s and 225s for a vertical field with maximum field of 100G.

Wave Speed (km/s)	0G	50G	75G	100G
2Mm	12.6	96.5	47.7	25.2
1Mm	10.1	64.1	44.4	45.4
0.5Mm	8.7	45.4	37.8	32.3

Table 1. The table shows wave speeds obtained from the distance-time plots for the 300s period driver with magnetic fields of 0G,50G, 75G and 100G.

Magnetic Field (G)	1Mm	2Mm	4Mm	5.5Mm
0G	0.2625	0.0021	1.4846×10^{-6}	1.7399×10^{-6}
50G	0.5401	-4.9441	0.882	0.5417
75G	0.1978	-1.576×10^{-4}	1.1586×10^{-6}	8.1936×10^{-7}
100G	0.0165	-1.8664	0.7116	0.4092

Table 2. The table shows the time averaged and integrated energy flux ratio obtained for the 300s period driver with magnetic fields of 0G,50G, 75G and 100G.

the transition layer to the upper boundary of the model β has a constant value of 1×10^{-6}. It is anticipated that for the region with $\beta \approx 1$, mode conversion occurs with full or partial conversion to magnetohydrodynamic modes.

Figure 6 shows the vertical component of the velocity at various times for different sections through the simulation box. Each plot in figure 6 corresponds to a vertical field configuration with a maximum field strength (B_{max}) of 100G. Referring to Griffiths et al. (2018b), there is a clear difference between the purely hydrodynamic, 0G case and the MHD cases. The figures exhibit evidence of a fast moving magneto-acoustic wave mode. These figures compare the wave modes at a quarter, half and three-quarters of a cycle. The propagation speed is consistent with that of a fast magneto-acoustic mode. Our results indicated that even a small magnetic field appears to enhance the motion of plasma in the corona and there is an apparent difference in phase between the magnetic field cases. As well as an increase in the velocity amplitude with increasing magnetic field there is a small shift in the frequency of the oscillation. For magnetic fields with strengths between $1kG$ and$50G$, the theoretical prediction of Hindman et al. (1996) resulted in frequency shifts in the microhertz and nanohertz range, although this was a helioseismology prediction it provides insight into the mechanism of frequency shifts of waves in atmospheric magnetic structures.

The full set of videos for all the simulations performed have been made available on the digital media repository hosted by The University of Sheffield, see Griffiths et al. (2018a). Each video shows the value of the vertical component of the plasma velocity (z-component) along different slices through the simulation box. The scale shows the velocity in m/s. Each video is labelled using the magnetic field strength in Gauss.

A distance-time plot for the 300s period driver, with the 100G field is shown in figure 7. The wavespeeds computed from this distance-time plot are shown in table 1. The speeds for the 0G field are consistent with the speed of sound in the solar atmosphere, whilst the speeds for the non zero magnetic field are consistent with propagation speeds for magnetosonic modes.

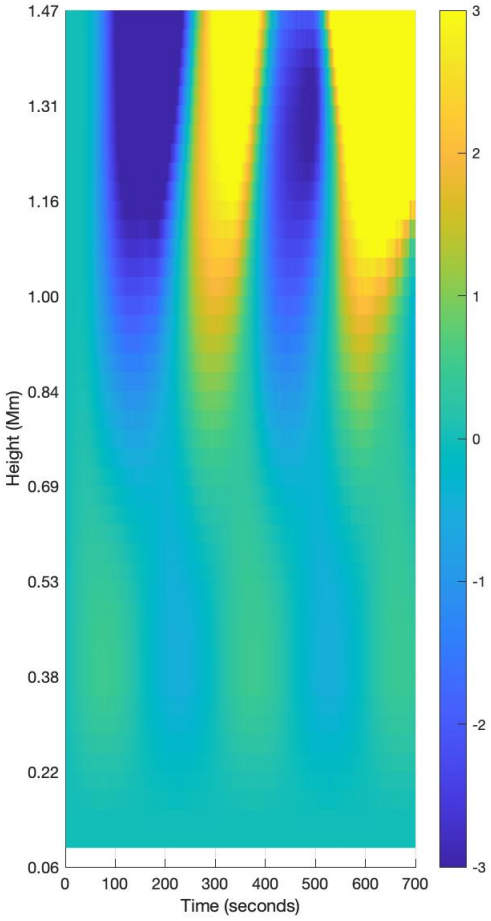

Figure 4. Distance-time plot of the vertical component of the velocity in the mid chromosphere.

In the lower region of the model atmosphere the simulations exhibit evidence of slow magnetoacoustic wave propagation perpendicular to the field lines. Since the source terms perturb only the vertical component of the velocity and the model is cylindrically symmetric, pure Alfvenic modes are not expected.

To determine how the propagation of the wave energy is influenced by the magnetic field strength, we compute the time averaged wave energy flux integrated over the cross-sectional area of the simulation box at different heights. The area of integration is perpendicular to the model z-axis.

$$F_{int} = \frac{1}{t_{max}} \int_0^{t_{max}} \int \mathbf{F}_{wave} \cdot d\mathbf{A} dt, \tag{11}$$

where the wave energy flux $\mathbf{F_{wave}}$ is given by

$$\mathbf{F}_{wave} = \tilde{p}_k \mathbf{v} + \tilde{\mathbf{B}} \cdot \mathbf{B}_b \mathbf{v} + \mathbf{v} \cdot \tilde{\mathbf{B}} \mathbf{B}_b.$$

The expression for the wave energy flux is dependent on the perturbed kinetic pressure, $\tilde{p}_k$, given by Bogdan et al. (2003)

$$\tilde{p}_k = (\gamma - 1) \left(\tilde{e} - \frac{(\tilde{\rho} + \rho_b) \mathbf{v}^2}{2} - \frac{\mathbf{B}^2}{2} \right).$$

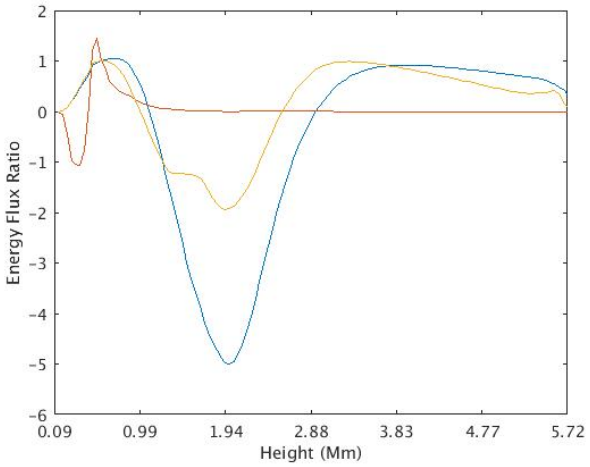

Figure 5. Shows the Ratio of the Integrated Energy Flux ratio for different values of the field, Blue 50G, Orange 75G, Red 100GMm

Using equation (11), we computed the energy flux integral for each of the drivers at different atmospheric heights and averaged over the total time. We compute the ratio of this integrated energy flux to the integrated energy flux at the location of the driver, the resulting values are shown in table 7.

With the exception of the 75G field case it appears that the energy flux is enhanced for increasing values for the vertical magnetic field. In figure 7 we plot the ratio of the integrated energy flux ratio for different values of the field at different heights and for the different vertical field values (the blue, orange and red are for field values of 50G, 75G and 100G respectively). This plot demonstrates that for higher B-field magnitudes the energy propagation is suppressed, this is interesting because this is consistent with observations and other simulation results which demonstrate an enhancement for inclined fields.

8. FREQUENCY ANALYSIS

The top panel of Figure 6 shows a vertical slice of Bz over time based on the simulation with the initial magnetic field configuration with a maximum value of 100 G. The vertical axis represents the height in Mm and the horizontal axis is the time dimension, measured in seconds. From this 2-dimensional plain, we selected 5 layers, indicated by vertical grey lines. The middle panel of Figure 6 displays the temporal variation of the selected layers, indicated by different grey shade colours. The time series do not feature non-stationary behaviour, therefore, further transformations (such as de-trending, smoothing or differentiation) are not needed, Although, Hanning-window function is still applied to avoid leakage effect when performing Fast Fourier Transformation (FFT).

FFT is applied (the lower panel) for investigating any oscillatory behaviour in the analysed signal. A significant oscillatory pattern is found with frequency range of 3.75 - 4 mHz, corresponding a period range of 4.2 - 4.4 minutes. FFT was also performed based on other simulations with different initial magnetic field configurations (with a maximum value of 0 G, 50 G 75 G and 100 G). These investigations all showed similar oscillatory behaviour, therefore, we present one FFT as a representative example.

Next, temporal analysis for observational data is performed for confirming the obtained oscillatory behaviour. We investigate intensity oscillations in the solar atmosphere observed by SDO/AIA. The passband 1600 Å is selected because our simulation mainly focuses on lower atmospheric regions, i.e. photosphere and chromosphere. The cadence of 1600 Å images is 24 seconds, therefore it is suitable for studying relatively high-frequency oscillations such as the obtained 4 mHz.

The initial magnetic field configuration of our model is a standing magnetic tube, passing through the chromosphere and the lower corona. Therefore, We chose to sample a typical active region. The selected area contains a small sunspot (solar pore), presumably featuring similar magnetic structure as our simulation. From each observation, a single pixel is selected, yielding a 0.35 Mm by 0.35 Mm area. The obtained time series shows non-stationary behaviour, therefore, the observed linear trend is removed by taking the first difference Δy_t of the data. The first difference is defined as

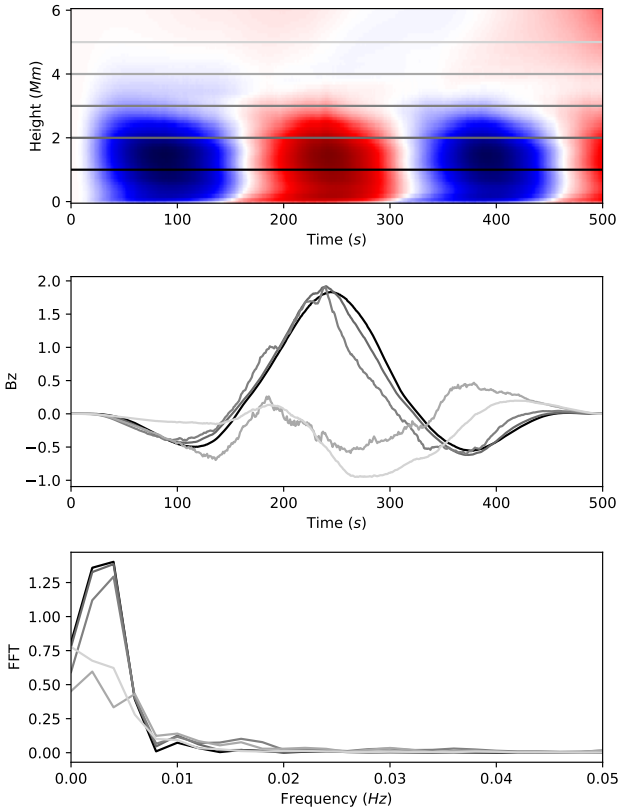

Figure 6. Temporal analysis of Bz vertical slices at 2 Mm. The top panel shows the selected vertical slices, indicated by gray colours. The middle panel demostrates the obtained signal after applying a Hanning window function. The bottom panel shows the result of the FFT analysis based on the 5 selected vertical Bz slices.

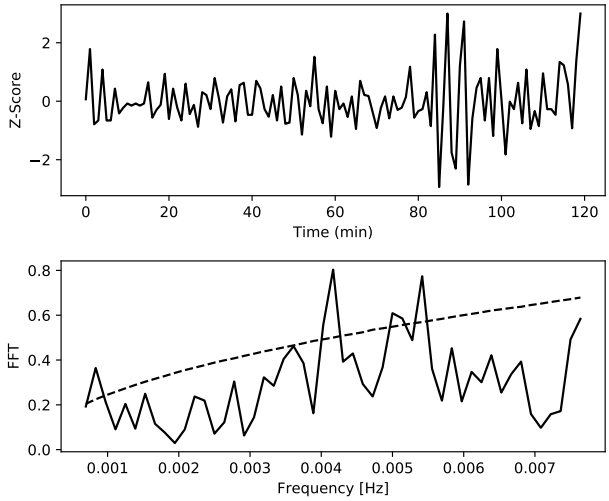

Figure 7. Temporal analysis of pixel intensity based on AIA 1600Å between 18:00 UT to 20:00 UT on 22 August 2010. The upper panel shows the temporal variation of the Z-Score (detrended and normalised pixel intensity data). The lower panel shows the FFT of the analysed observational data.

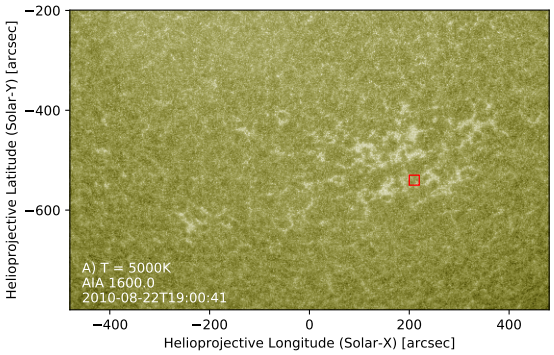

Figure 8. The selected pixel from the start of the investigate time series at 18:00 UT on 22 August 2010. The pixel is indicated by red rectangle.

the the difference between consecutive observations y_t and y_{t-1}. Furthermore, the times series is also normalised by applying standard scores (Z-scores), defined by:

$$Z_i = \frac{T_i - \overline{T}}{\sigma(T)}, \tag{12}$$

where, the parameter $\overline{T}$ is the mean of the time series and the parameter $\sigma(T)$ is defined as the standard deviation of the data. The top panel of Figure 6 demonstrates the trend removed and normalised time series. The lower panel of Figure 6 shows the result of the applied FFT technique. The dashed line is the significance level (3σ) which is calculated by Monte-Carlo method. The original data showed red noise signature which transformed to blue noise after differentiating the data. We have generated 1 million blue noise signatures N_b and calculated the standard deviation $\sigma(N_b)$ and the mean $\overline{N_b}$ of the simulated noise, providing our significance level S:

$$S = \overline{N_b} + 3\sigma(N_b). \tag{13}$$

A significant period is found with frequency range of $4 - 4.2\ mHz$, corresponding a period range of 4 - 4.2 minutes, which is close to the period found in simulation data. Another significant peak is found with period around 3 minutes which may be an indication of another global oscillation.

9. CONCLUSION

In this paper we have presented results for a series of MHD simulations of an extended oscillator at the base of a model solar atmosphere. We have shown that energy is propagated by magnetosonic modes. Slow and fast magnetosonic modes are responsible for carrying some energy back to the chromosphere and the photosphere. The results exhibit a small frequency shift for different values of the magnetic field closer inspection of the energy flux propagation results indicative of enhanced energy flux propagation for inclined magnetic fields. The obtained periodic behaviour is confirmed by observational data, featuring similar frequencies based on the intensity times series of SDO images. The frequency shift measured from the temporal analysis of the observational and simulation data is larger than would be expected from the analysis of Hindman et al. (1996). This can be understood in part by referring to the work of Campbell and Roberts (1989).

It is encouraging that the results presented here are consistent with the behaviour exhibited by earlier work. Future work will address simulation runs over longer time periods and for inclined fields. There is an issue that due to the extended nature of the driver the amplitudes used may be responsible for delivering vast quantities of energy into the solar atmosphere and for driving a highly numerically unstable system and inducing extremely large shocks Calvo Santamaria, Khomenko and Collados (2015).

10. ACKNOWLEDGMENTS

The authors thank P. H. Keys for providing the wavelet tools to analyse the related SDO data M.Korsos for the preparation of Figure 1, the Science and Technology Facilities Council (STFC) for the support they received. RE

acknowledges the support received from the the Royal Society (UK). We acknowledge IT Services at The University of Sheffield for the provision of the High Performance Computing Service.

Software: SMAUG (Griffiths et al. 2015), SAC (Shelyag et al. 2008), VAC (Tóth 1996)

REFERENCES

Bogdan, T. J., Carlsson, M., Hansteen, V. H., McMurry, A., Rosenthal, C. S., Johnson, M., Petty-Powell, S., Zita, E. J., Stein, R. F., McIntosh, S. W., Nordlund, Å., 2003. Waves in the Magnetized Solar Atmosphere. II. Waves from Localized Sources in Magnetic Flux Concentrations. ApJ599, 626–660.

Calvo Santamaria, I., Khomenko, E., and Collados, M., 2015. Magnetohydrodynamic wave propagation from the subphotosphere to the corona in an arcade-shaped magnetic field with a null point. A&A577, A70.

Campbell, W. R. and Roberts, B. 1989. The Influence of a Chromospheric Magnetic Field on the Solar p- and f-Modes ApJ, 338, 538. doi:10.1086/167216

Carlsson, M., Stein, R. F., 1995. Does a nonmagnetic solar chromosphere exist? ApJL440, L29–L32.

Caunt, S. E., Korpi, M. J., Apr. 2001. A 3D MHD model of astrophysical flows: Algorithms, tests and parallelisation. A&A369, 706–728.

Fedun, V., Erdélyi, R., Shelyag, S., Sep. 2009. Oscillatory Response of the 3D Solar Atmosphere to the Leakage of Photospheric Motion. SoPh258, 219–241.

Fedun, V., Erdélyi, R., Shelyag, S., Sep. 2009. MHD waves generated by high-frequency photospheric vortex motions. Annales Geophysicae 29, 1029-1035.

Griffiths, M. K., Fedun, V., Erdélyi, R., 2015. A Fast MHD Code for Gravitationally Stratified Media using Graphical Processing Units: SMAUG. Journal of Astrophysics and Astronomy 36, 197–223.

Griffiths, M., Erdélyi, R., Fedun, V., 2017. Videos of Magnetohydrodynamics Simulations of Solar Atmosphere Wave Dynamics Generated by Solar Global Oscillating Eigenmodes. https://figshare.com/articles/Videos_of_Magnetohydrodynamics_Simulations_of_Solar_Atmosphere_Wave_Dynamics_Generated_by_Solar_Global_Oscillating_Eigenmodes/4818490

Griffiths, M., Erdélyi, R., Fedun, V., 2018. Videos of p-Mode Oscillations in Highly Gravitationally Stratified Magnetic Solar Atmospheres. https://figshare.com/articles/Videos_of_Magnetohydrodynamics_Simulations_of_Solar_Atmosphere_Wave_Dynamics_Generated_by_Solar_Global_Oscillating_Eigenmodes/4818490

Griffiths, M. K., Fedun, V., Erdélyi, R., and Zheng,R., Solar atmosphere wave dynamics generated by solar global oscillating eigenmodes.Advances in Space Research, 61: 720–737, January 2018.

B. V. Gudiksen, M. Carlsson, V. H. Hansteen, W. Hayek, J. Leenaarts, and J. Martínez-Sykora. The stellar atmosphere simulation code Bifrost. Code description and validation. *A&A*, 531:A154, July 2011. https://doi.org/10.1051/0004-6361/201116520.

Hindman, B. W. and Zweibel, E. G. and Cally, P. S., Mar. 1996. Driven Acoustic Oscillations within a Vertical Magnetic Field. ApJ459, 760–772.

Kalkofen, W., 2012. The Validity of Dynamical Models of the Solar Atmosphere. SoPh276, 75–95.

Khomenko, E., Calvo Santamaria, I., 2013. Magnetohydrodynamic waves driven by p-modes. Journal of Physics Conference Series 440 (1), 012048.

I. Kontogiannis, G. Tsiropoula, and K. Tziotziou. Power halo and magnetic shadow in a solar quiet region observed in the Hα line. *A&A*, 510:A41, February 2010. https://doi.org/10.1051/0004-6361/200912841.

Leenaarts, J., Carlsson, M., Hansteen, V., Gudiksen, B. V., 2011. On the minimum temperature of the quiet solar chromosphere. A&A530, A124.

Leighton, R. B., 1960. In: Thomas, R. N. (Ed.), Aerodynamic Phenomena in Stellar Atmospheres. Vol. 12 of IAU Symposium. pp. 321–325.

Malins, C., 2007. On transition region convection cells in simulations of {p}-mode propagation. Astronomische Nachrichten 328, 752–755.

McWhirter, R. W. P., Thonemann, P. C., Wilson, R., 1975. The heating of the solar corona. II - A model based on energy balance. A&A40, 63–73.

Murawski, K., Zaqarashvili, T. V., 2010. Numerical simulations of spicule formation in the solar atmosphere. A&A519, 9.

Shelyag, S., Fedun, V., Erdélyi, R., 2008. Magnetohydrodynamic code for gravitationally-stratified media. A&A486, 655–662.

Tóth, G., 1996. A General Code for Modeling MHD Flows on Parallel Computers: Versatile Advection Code. Astrophysical Letters and Communications 34, 245.

Vernazza, J. E., Avrett, E. H., Loeser, R., 1981. Structure of the solar chromosphere. III - Models of the EUV brightness components of the quiet-sun. Astrophysical Journal Supplement Series 45, 635–725.

Vigeesh, G.,Fedun, V.,Hasan, S. S., Erdélyi, R., Jan. 2012. Three-dimensional Simulations of Magnetohydrodynamic Waves in Magnetized Solar Atmosphere. ApJ755, 1–18.

A. Vögler, S. Shelyag, M. Schüssler, F. Cattaneo, T. Emonet, and T. Linde. Simulations of magneto-convection in the solar photosphere. Equations, methods, and results of the MURaM code. *A&A*, 429: 335–351, January 2005. https://doi.org/10.1051/0004-6361:20041507.